Chapter 5

Observations of Supernova Remnants

This chapter discusses the GMRT 325-MHz observations of candidate and known SNRs. The motivation behind this exercise was two-fold. Firstly, to use the higher sensitivity and resolution provided by GMRT at low frequencies which would unambiguously identify the SNRs. Secondly, GMRT has only recently come to a stage where enough antennas are available in the interferometric mode to attempt imaging of weak extended sources, which truly tests the imaging performance of the instrument. In these early stages of the telescope where a large fraction of time and effort goes into debugging the instrument, it was important to have a scientific goal in mind to provide the focus, direction and motivation to debug the telescope and bring it to a level where it can be used for scientific purposes. These observations provided the required focus where the scientific returns for the debugging effort put-in were perceived to be substantial.

5.1 Introduction

Radio emission from Supernova remnants (SNRs) is due to the synchrotron radiation mechanism which has a non-thermal power law dependence on frequency with a negative spectral index α ($S \propto \nu^{\alpha}$). This makes the emission progressively stronger at lower frequencies (see Section 1.1). On the other hand, thermal emission from typical HII regions, the other class of objects with extended radio emission in the Galaxy, has a flat spectrum above ≈ 1 GHz. Below this frequency, the optical depth is much greater than 1 and the spectrum turns over with a spectral index of 2. The low frequency continuum spectra of Galactic objects are therefore frequently used to distinguish between thermal and non-thermal sources of emission (Kassim et al. 1989a; Kassim & Weiler 1990; Subrahmanyan & Goss 1995). The other key observational evidence used to identify SNRs is their morphology. Detection of an extended non-thermal source with no thermal emission has been the criterion used to identify Galactic sources as SNRs.

Kassim (Kassim 1989), in a study of non-thermal emission from known Supernova remnants in the Galaxy, demonstrated that the radio emission from most SNRs gets absorbed at frequencies below about 100 MHz. He observed a number of SNRs, widely distributed in the inner Galaxy and showed that about two thirds of all SNRs show this spectral turn-over due to free-free absorption by the intervening ISM; this indicates the presence of an extended low density warm ionized medium (ELDWIM) in the Galaxy. Since then, many more SNRs has been imaged at frequencies between 1 GHz and 327 MHz (and in some cases even below 327 MHz). A collection of the radio spectra of SNRs have been compiled by Trushkin (1998)[1]. His catalogue of SNR spectra also gives the spectral indices above and below the turn-over frequency and the frequency at which the spectrum turns over. Spectra of about 35% of the SNRs from this catalogue show a low frequency turn-over. The measurement of this turn-over frequency for SNRs distributed throughout the Galaxy can be used to indirectly measure the distribution of this phase of the ISM, which is otherwise inaccessible to direct observations.

Imaging of HII regions at frequencies below ~ 1 GHz, together with the electron temperature derived from RRL observations have been used to deduce improved estimates of the physical properties of HII regions (Shaver 1969; Subrahmanyan 1992b,a; Kassim et al. 1989b). Low frequency continuum mapping in the Galactic plane is therefore important from the point of view of identification of SNRs, separating thermal emission from non-thermal emission and for studying the intervening ISM.

Radio emission from SNRs is typically extended, often with a low surface brightness. Telescopes which are sensitive to extended emission as well as to total flux, are required to image such objects. Single dish observations are sensitive to emission at all scales in the field. While interferometric telescopes typically provide much higher resolution, they are insensitive to scales larger than those corresponding to the smallest projected baseline. Single dish telescopes, at high frequencies, provide the sensitivity and moderate resolution required for such work. Till recently many observations were therefore done using single dish instruments. However, single dish observations pose a separate problem.

[1]Available from http://www.ratan.sao.ru/~cats on the web

While single-dish observations do not discriminate against extended emission, they are more prone to large scale confusing emission, which is abundantly present in the Galactic plane. Low frequency single dish observations do not provide the required resolution to resolve the extended nature of the SNR emission. For these reasons, most Galactic SNRs have been observed using single dishes at high frequencies (> 1 GHz) which provide reasonable resolution (better than $1'$). Higher resolution interferometric observations of some Galactic SNRs have also been done. However, such observations are often restricted to observing relatively small sized SNRs. Imaging at low frequencies using interferometers is also relatively difficult due to problems arising from higher level of RFI, higher phase noise at low frequencies (due to various reasons ranging from cross talk to ionospheric phase corruption), non-co-planarity of array requiring much more complex software and higher computing power. Hence, even interferometric observations have been typically done at frequencies > 1 GHz.

However, observations at high frequencies have another source of emission, namely the thermal emission from HII regions which, in some cases, is fairly strong. The non-thermal emission from SNRs becomes progressively diminished at higher frequencies, while the thermal emission remain fairly constant as a function of frequency at frequencies higher than about 1 GHz. High frequency observations therefore miss extended low surface brightness emission from SNRs. Such observations alone can also wrongly classify sources which have thermal and non-thermal components in the radiation (for example, due to line-of-sight super-position of thermal and non-thermal emission). Thus, while high frequency telescopes provide the required resolution and sensitivity, they alone are not adequate for the identification of Galactic objects as SNRs.

Recently, synthesis telescopes like the GMRT (Bhatnagar 2000) and MOST (Gray 1994a) have been used to image parts of the Galactic plane. The MOST survey, at a resolution of $\approx 90 \times 43.5 \text{ arcsec}^2$ and is sensitive to angular scales up to $30'$, identified seventeen candidate SNRs. Most of these object are large ($> 5 - 10'$). Many of the fields however suffer from the grating response due to nearby strong sources and from confusing thermal emission from nearby strong HII regions.

Duncan et al. (1997b) used the Parkes 64-m single dish telescope to image a set of large, high latitude SNRs at 2.4 GHz. These observations identified about a dozen new large SNRs ($> 15'$) south of $-25°$ declination. Again, besides the lower angular resolution of the single dish, these observations suffered from the problem of separating extended diffused non-thermal emission from thermal emission in and around the Galactic plane

Table 5.1: Observed and derived physical parameters of the candidate SNRs in the fields. Type code 'S' implies shell-type, 'B' implies barrel-type while 'N' means that the object is most likely not an SNR.

Name	RA_{J2000} ($h\ m\ s$)	Dec_{J2000} ($^\circ\ '\ ''$)	S_{327MHz} (Jy)	Size (arcmin)	Type	α ($S \propto \nu^{\alpha}$)
G001.4−0.1	17 49 39	-27 45	4.2 ± 0.5	8.0	S	-0.8 ± 0.3?
G003.7−0.2	17 55 29	-25 50	4.5 ± 0.3	-	B	-0.7 ± 0.1
G003.8+0.3	17 53 02	-25 24	8.7 ± 0.3	18	S	-0.9?
G004.2−0.0	17 55 22	-25 15	0.1 ± 0.2	-	N	-
G004.8+6.2	17 33 24	-24 34	5.5 ± 1.2	17	S	-0.6 ± 0.1
G356.2+4.5	17 18 58	-29 40	8.1 ± 1.7	25	S	-0.7 ± 0.2
G356.3−1.5	17 42 40	-32 52	5.7 ± 0.2	15	S/B	$> -0.7 \pm 0.1$
G358.0+3.8	17 26 03	-28 36	2.5 ± 1.3	37×39	S	-

using these high frequency.

The GMRT at 327 MHz provides a resolution of up to ~ 20 arcsec and is sensitive to spatial scales up to 30 arcmin. The relatively smaller field-of-view (half-power beam width of $\approx 1^\circ.4$) of the GMRT also provides an advantage in terms of attenuating confusing emission from near by strong sources. At this frequency, the thermal emission from typical HII regions is severely diminished, while the emission from SNRs remain relatively strong. The higher resolution and sensitivity at these low frequencies, make the GMRT an ideal instrument for studies of Galactic SNRs. Compared to the resolutions of about $1'$ and $1.5'$ and RMS noise of ≈ 20 mJy/beam and 35 mJy/beam in the survey by Duncan et al. (1997b) and Gray (1994a) respectively, the GMRT at 327 MHz provides a factor of 2 lower RMS noise and, depending upon the largest baselines used, up to 2–5 times better resolution.

5.2 Candidate SNRs

This section presents the results from the 327-MHz GMRT observations of fields containing candidates SNRs. The list of fields observed and the parameters of SNRs found in these fields are list in Table 5.2.

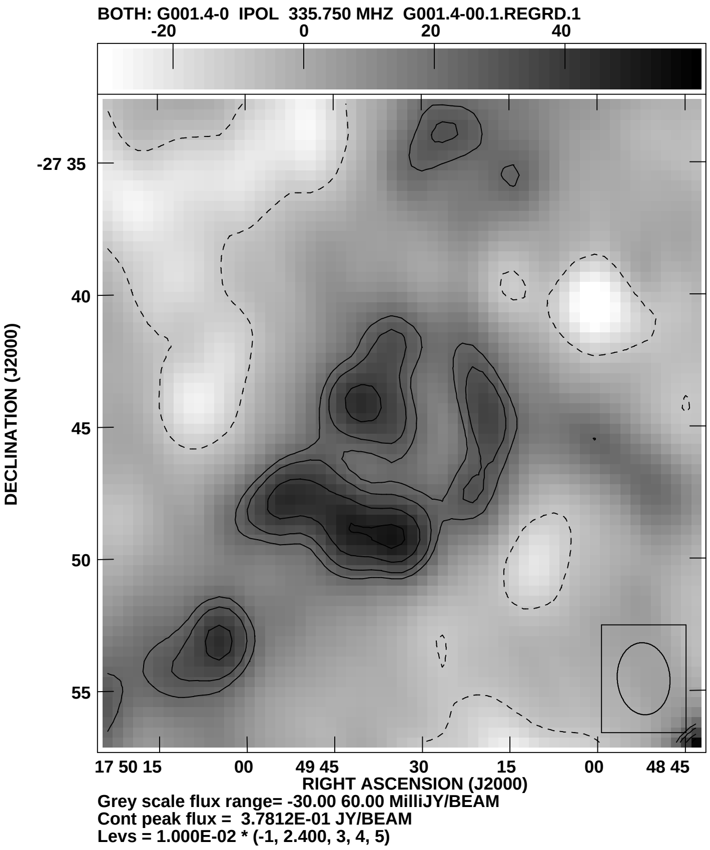

Figure 5.1: 327-MHz image of G001.4−0.0 using GMRT. A partial shell with compact source located almost at the centre is clearly detected.

5.2.1 G001.4−0.1

The GMRT 327-MHz image of G001.4−0.0 is shown in Fig. 5.1. A partial arc of ~ 8 arcmin diameter is clearly visible in this image. A compact source, almost at the geometric centre of the arc is also clearly visible. The morphology is very similar to that of the nearby composite SNR G000.9+0.1 which has a flat spectrum, X-ray emitting compact central source (Mereghetti et al. 1998). This SNR lies just north-east of the Sgr D HII region and at the very edge of the VLA 327-MHz wide-field image of the Galactic centre region (LaRosa et al. 2000). A weak fuzz of emission is seen in this wide-field image corresponding to this SNR. However, the image quality for this region is too poor (due to primary beam attenuation) to be able measure the flux density or decipher the morphology.

The 327-MHz flux density measured from our observation was found to be 4.2 ± 0.5 Jy. The 843-MHz image (Gray 1994a) suffers from artifacts due to the grating response of

Sgr A and the flux density of $\sim$ 2 Jy is hence only a "tentative" figure. From their 1616 MHz VLA observations of this region, Liszt (1992) reported "an arc of incomplete shell" of diameter $\sim$ 7 arcmin at this location. The incomplete arc seen in the GMRT image agrees well with the incomplete arc seen in the 1616-MHz image. The MOST image of this object shows a relatively featureless source of emission and the "complete shell" reported by Gray (1994a) is difficult to decipher.

This source was also the target of observations for the detection of OH (1720 MHz) maser emission by Yusef-Zadeh et al. (1999). In the VLA A-array observation, they detect a maser spot, coincident with the western edge of the arc. Their VLA D-array observations detect an extended arc of emission, almost coincident with the arc seen in the radio continuum images.

The spectral index between 327 and 843 MHz is -0.8 ± 0.3 for the shell. However, given that the 843-MHz flux density is quite uncertain, this value of the spectral index remains tentative and is used only to show the non-thermal nature of emission. Based on the morphology, non-thermal nature of emission and association of OH (1720 MHz) emission, we propose that this is a shell-type SNR in the Galactic plane.

5.2.2 G003.8+0.3

Gray (1994a) describes G003.8+0.3 as a "fairly weak, incomplete ring structure most perfectly centered on a slightly extended source". The morphology of this object in the GMRT 327-MHz image, shown in Fig. 5.2, matches well with the 843-MHz MOST image. This SNR is also in the field of view for the pointings for G003.7−0.2 and G004.2−0.0. The partial shell is clearly visible in both the images. The IRAS 60μm image, shown in Fig. 5.3, does not show any significant emission at this position. However, this SNR lies within a ring of IR emission seen clearly in this image. The northern rim of the radio ring is significantly brighter and more extended, almost filling the IR ring, making it difficult to define the center of the radio ring structure. The "central source" in the radio image is fairly close to the center defined by the inner edge of the ring structure, but not close to the center defined by the outer edges. The bridge of emission connecting the central source and the ring is not so clearly seen at 327 MHz.

The integrated flux density of this region at 327 MHz is 8.7 ± 0.3 Jy. The diameter of the ring structure (including the northern extension) is $\approx 18'$ while its center is at $\mathrm{RA}_{J2000} = 17^h53^m02^s$, $\mathrm{Dec}_{J2000} = -25°24'$. The position of the emission peak for the 'central source' is $\mathrm{RA}_{J2000} = 17^h52^m54^s$, $\mathrm{Dec}_{J2000} = -25°28'$. The flux density of the VLA

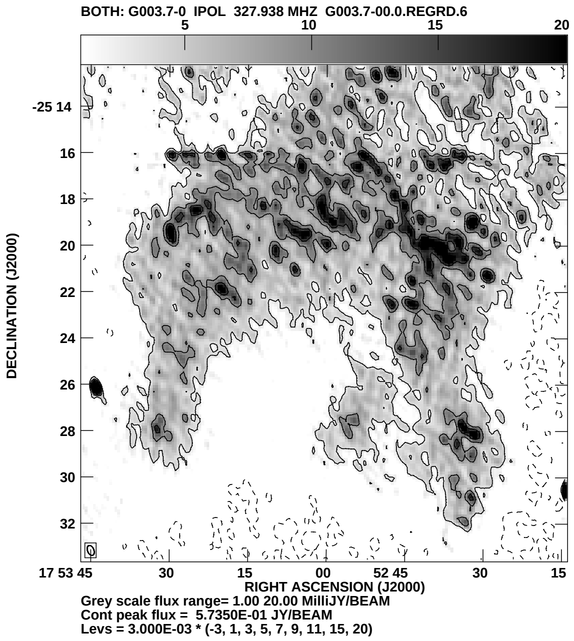

Figure 5.2: GMRT image at 325 MHz of G003.8+0.3. The shell morphology of G003.8+0.3 is clearly visible.

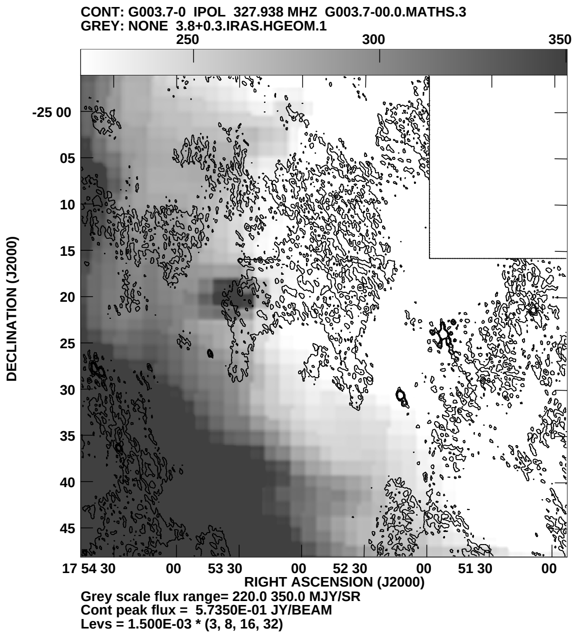

Figure 5.3: 327-MHz contours overlayed on the 60μm IRAS gray scale image of G003.8+0.3. A shell of IR emission is visible and the radio emission from the SNR is completely within the IR shell and almost fills the IR shell in the north. There is, however, no significant IR emission at the location of the SNR itself. The small extension in the eastern edge of the radio shell is coincident with the strong IR compact source.

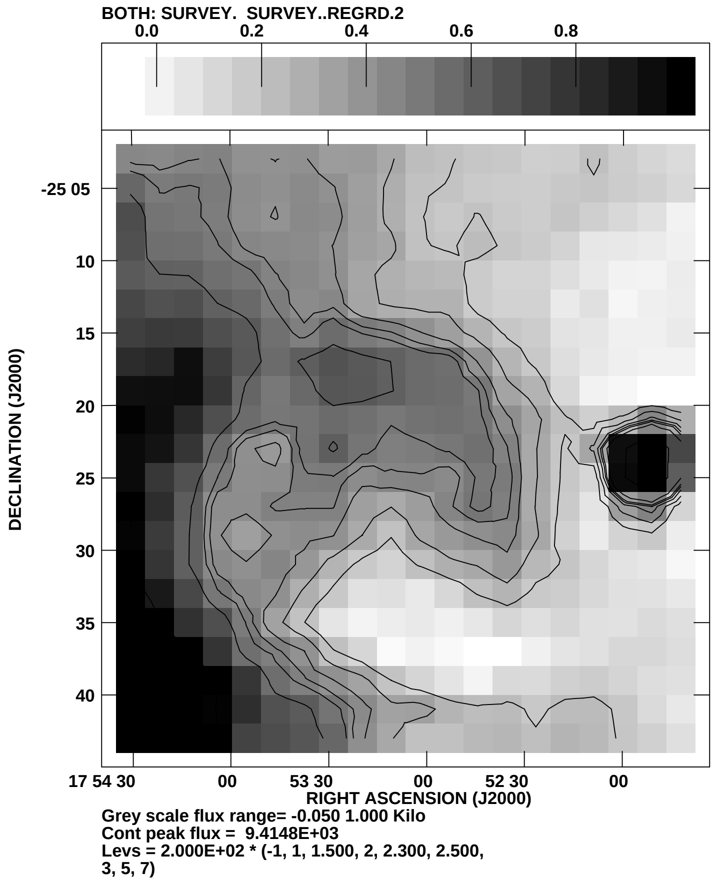

Figure 5.4: Image of G003.8+0.3 at 11 cm from the 100-m Effelsberg single dish survey. An arc of emission similar to that seen at lower frequencies is clearly visible.

21-cm calibrator $J1751-253$, which is just west of this region is measured to be 1.3 ± 0.2 Jy. Flux density of this source from Texas survey (Douglas et al. 1996) is $1.41 \pm .09$ Jy.

The flux density reported by Gray (1994a) at 843 MHz is ≈ 3.5 Jy giving a spectral index of -0.9. Based on the morphological evidence and evidence for non-thermal nature of emission, we propose that this source is a weak, Galactic SNR.

The 'central source' is detected as a point source at 1400 MHz in the NRAO-VLA All Sky Survey (NVSS) with a flux density of 15.1 mJy. Although it is a weak source in the 327-MHz image with flux density barely at the 2σ level, it is nonetheless stronger than 15 mJy, proving that it is a non-thermal source. With a large error in the measurement of the 327-MHz flux density, it is difficult to determine an accurate spectral index.

Image of this SNR from the radio continuum survey of the Galactic plane at 11 cm using the 100-m Effelsberg telescope (Reich et al. 1990) is shown in Fig. 5.4. Here too, a partial shell of emission is visible, which matches well with the morphology of this SNR seen at 843 and 327 MHz. Significant amount of linear polarization is also detected in the 11 cm polarized images.

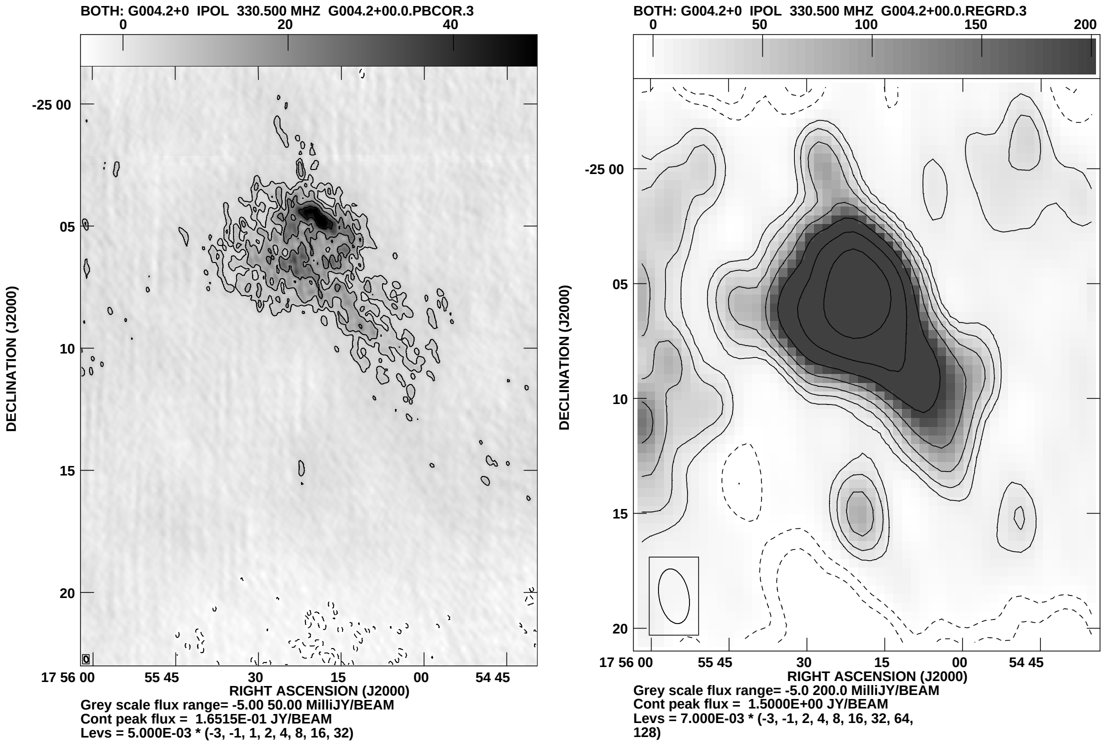

Figure 5.5: GMRT 327-MHz image of the region containing G004.2+0.0. The strong extended source in this field is a classified Ultra Compact H II region G004.417+0.126. The left panel shows the high resolution image ($\sim 15 \times 11$ arcsec^2) of this region where the core-halo morphology of G004.417+0.126 is clearly visible. It's south-western tail is visible in Grey's 843-MHz image of this region. The RMS noise in the map is about 5 mJy/beam. The right panel shows the low resolution image where an unresolved source is detected at the location of the candidate SNR just south of G004.417+0.126. The RMS noise in this image is ~ 8 mJy/beam.

5.2.3 G004.2−0.0

This source is the smallest diameter candidate SNR (size ~ 3.5 arcmin) reported by Gray (1994a). He reported the location of this object as $\mathrm{RA}_{J2000} = 17^h 55^m 17^s, \mathrm{Dec}_{J2000} = -25°14'51''$. The total 843-MHz flux density was reported to be 200 mJy. However this ob-

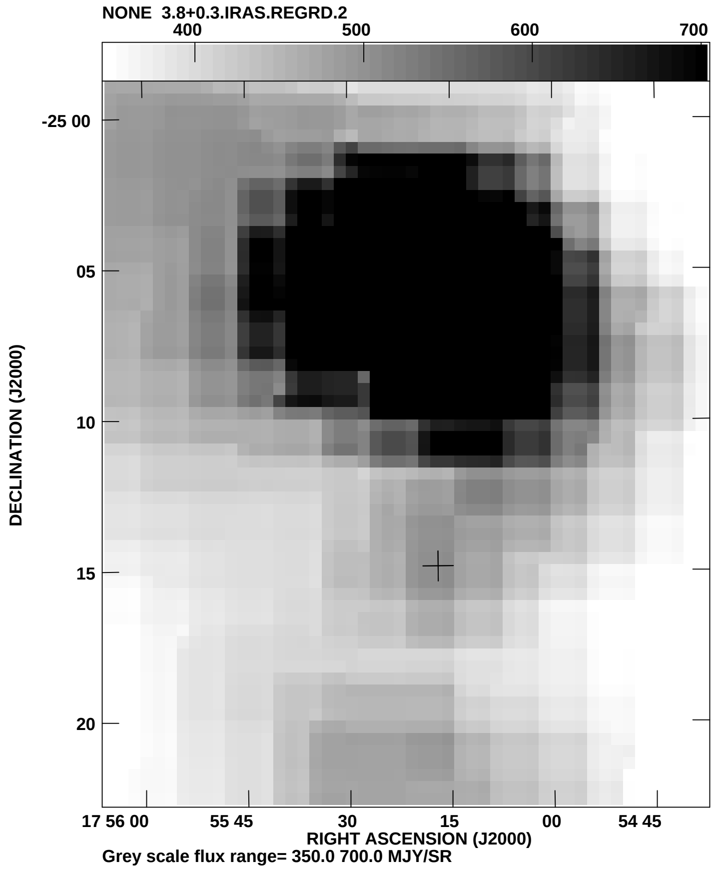

Figure 5.6: The IRAS 60μm image of the region containing G004.2+0.0. The strong source seen just north of G004.2+0.0 in the GMRT 327-MHz image is the strongest source in the IRAS image. A faint source, indicated by a cross at the position of G004.2+0.0 is also detected in this IRAS image.

ject sits in a negative bowl and the measured value after tentative correction for this bowl is in the range of $100 - 300$ mJy (Gaensler, private communication). A high resolution image of this field was made to look for the shell-type structure at 327 MHz. There is a hint of a compact source in this image at $\mathrm{RA}_{J2000} = 17^h55^m22^s, \mathrm{Dec}_{J2000} = -25°15'01''$, but barely at the 2σ level. No shell-type structure was detected at the level of ~ 5 mJy/beam with a resolution of ~ 15 arcsec. The low resolution image, shown in Fig. 5.5 has a ~ 100 mJy object at the location of this source. There is probably a compact source in the NVSS image at this location, but again at the $1 - 1.5\sigma$ level. The $60\mu m$ IRAS image of this region (Fig. 5.6) also shows significant extended emission at the location of this source (indicated by a cross in the figure), which appears to be associated with the HII region in the north, indicating that this may be a thermal source. This source, based on the available radio flux densities is therefore consistent with it being a flat spectrum thermal source and may not be an SNR.

The dominant extended source in the image shown in Fig. 5.5 is a known HII region, G004.4+0.1 located at $\mathrm{RA}_{J2000} = 17^h55^m26^s, \mathrm{Dec}_{J2000} = -25°05'08''$ (Kuchar & Clark 1997). A compact core surrounded by a halo of lower surface brightness is clearly visible in this image and this core-halo morphology is suggestive of this being a compact HII region (Wood & Churchwell 1989b). In combination with high resolution images at other frequencies, these data can provide information about the physical conditions in this HII region.

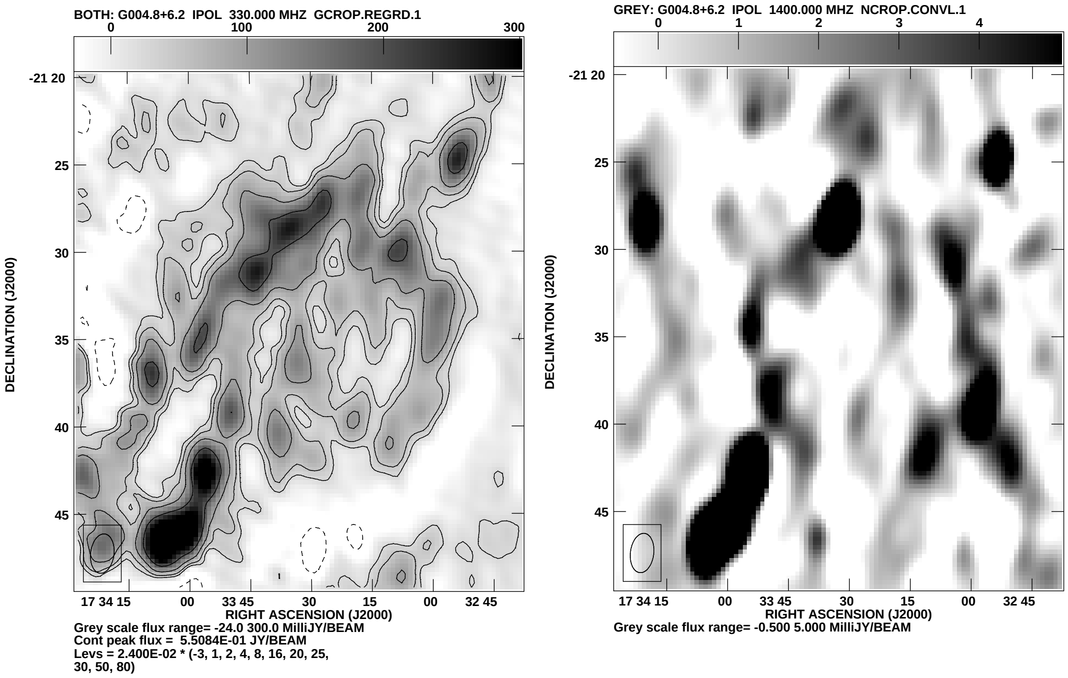

Figure 5.7: GMRT image of G004.8+6.2 at 327 MHz and NVSS image at 1400 MHz. The resolution in the GMRT image is $2.2' \times 1.3'$ along PA $-07°$ and the RMS noise is 23 mJy/beam. The NVSS image has been smoothed to the resolution of the GMRT image and has a RMS noise of 0.5 mJy/beam.

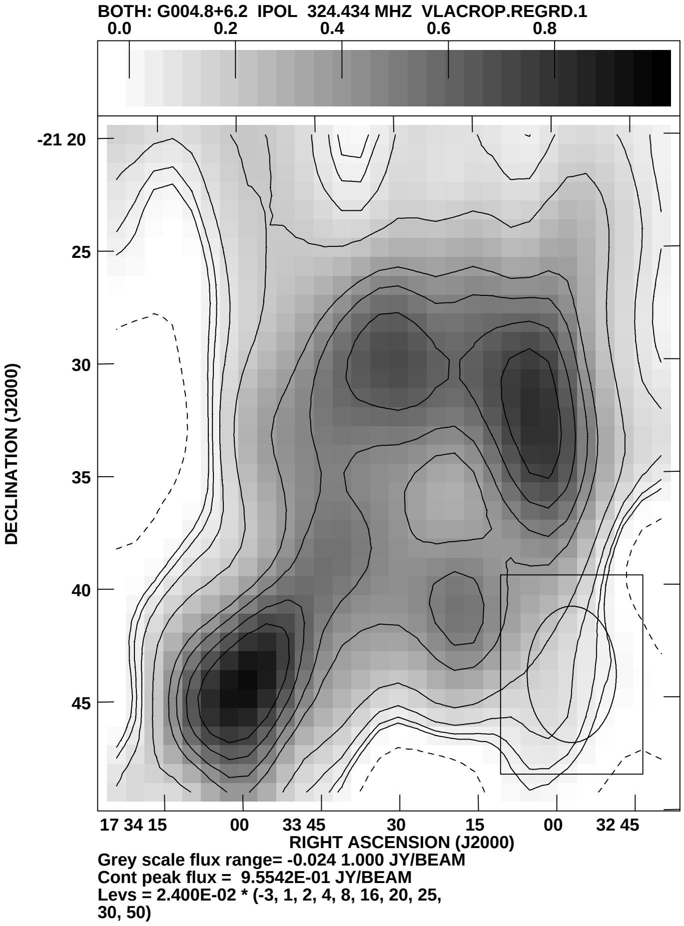

Figure 5.8: VLA image of G004.8+6.2 at 325 MHz. The resolution in this image is $6' \times 4'$ along PA $-0.8°$ and the RMS noise is 24 mJy/beam.

5.2.4 G004.8+6.2

Fig. 5.7 shows the GMRT 327-MHz and NVSS 1400-MHz images of G004.8+6.2 (formerly designated as G004.5+6.2). This object of size $17' \times 18'$ is located $40'$ east of Kepler's SNR (Fig. 5.14). The total flux density at 327 MHz is 5.5 ± 1.2 Jy and the co-ordinates of the center of the ring are $\mathrm{RA}_{J2000} = 17^{\mathrm{h}}33^{\mathrm{m}}24^{\mathrm{s}}$, $\mathrm{Dec}_{J2000} = -21°34'$. The apparent flux density of Kepler's SNR in the GMRT image before primary beam correction was approximately 20 percent lower than the value of 38 Jy after primary beam correction. The integrated flux density of G004.8+6.2 at 2.4 GHz was reported to be 1.3 ± 0.2 Jy and the value at 4.85 GHz from PMN image of this region was found to be 1.12 ± 0.07 Jy, which gives a spectral index of -0.57 ± 0.13. The NVSS image shows a well resolved ring coincident with the emission at 327 MHz. Since NVSS misses most of the extended emission, we did not attempt to use the NVSS flux density to determine the spectral index of the source. We attribute the lower signal-to-noise ratio in this map to the presence of side lobes of the synthesized beam from Kepler's SNR contaminating the entire map. It could also be partly due to the non-isoplanacity of the ionosphere at these scales as well as pointing errors in the antennas.

This SNR was also in the field of view of a VLA D-array multiple snap-shot observation at 325 MHz in March 1999. This observation was part of another project not included in this dissertation to make continuum images of Galactic SNRs at 325 and 74 MHz to get reliable low frequency spectra and, wherever possible, spectral index maps. The image from these observations is shown in Fig. 5.8. The resolution is $6' \times 4'$, but the image is in good agreement with the higher resolution GMRT image. The integrated flux density from the VLA 327-MHz image is 4.9 ± 1.3 Jy, which is consistent with the flux density from the GMRT image within the errors bars.

5.2.5 G356.3-1.5

This SNR is classified as a 'classic barrel' SNR by Gray (1994a) from the 843-MHz image. The GMRT 327-MHz image (Fig. 5.9) shows the basic structure seen in the 843-MHz image where the two edges are relatively brightened compared to the center of the remnant. However, at 327 MHz, the center is also filled with significant emission, not seen in the 843-MHz image. Although it does show the brightened rims (probably of the shell), which were seen as the dominant sources of emission in the 843-MHz image, there is no well defined minimum of emission in a direction perpendicular to these rims. Gaensler (1998) laid down the following criterion to classify a SNR as 'barrel' shaped:

1. It must be of the shell- or composite-class

2. The highest resolution image available must have a minimum of 10 beams across its diameter

3. It must have clear minima in emission separated by position angles of $180^\circ \pm 30^\circ$ relative to the assumed center of the SNR (this defines the axis of symmetry for the 'barrel').

4. It must have well-defined maxima and at approximately perpendicular position angles to the minima

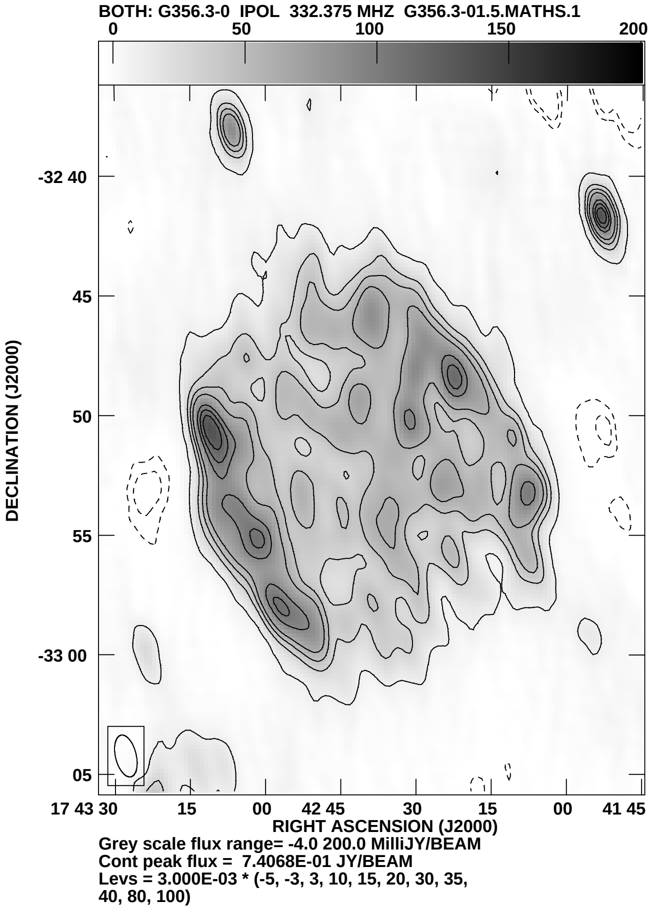

Figure 5.9: 327-MHz image of G356.3-1.5 using the GMRT. The box shaped morphology of the object is apparent. The emission filling the center of the object is not detected in the 843-MHz MOST image of Gray. The RMS noise in the image is 7 mJy/beam and the total flux density of the source is 5.7 ± 0.2 Jy

5. A clear bilateral axis should be identifiable, passing through the two minima and through the center of the SNR.

The clear minima along the circumference of an otherwise shell-type SNR makes its classification as a 'barrel' shaped secure. The 843-MHz image, where questionable data processing was done (namely, the subtraction of a smooth component to remove the effect of the grating response from a nearby strong source), shows a well defined minimum of emission between the two rims of emission which is filled by emission in the 327-MHz image. Although morphologically this central emission appears to be emission from the edges of the 'barrel' seen in projection, it is important to measure the spectral index of this emission to evaluate the possibility of this being a filled-center SNR. With a size of $\approx 15'$, this can be reliably mapped at 610 and 233 MHz with the GMRT.

The integrated flux density measured at 332 MHz from the GMRT image is 5.7 ± 0.2 Jy. The RMS noise in the image in the vicinity of this object is about 4 mJy/beam. The integrated flux density in the modified image at 843 MHz is reported to be 2.8 Jy. This implies a spectral index of -0.7 ± 0.1 between 843 and 332 MHz. However the 843-MHz image is marred by a grating response due to G357.7-0.1 and a smooth model of this artifact has been removed, though not entirely successfully (as reported by Gray (1994a)). The 843-MHz flux density is therefore likely to be under estimated and the resulting spectral index an upper limit.

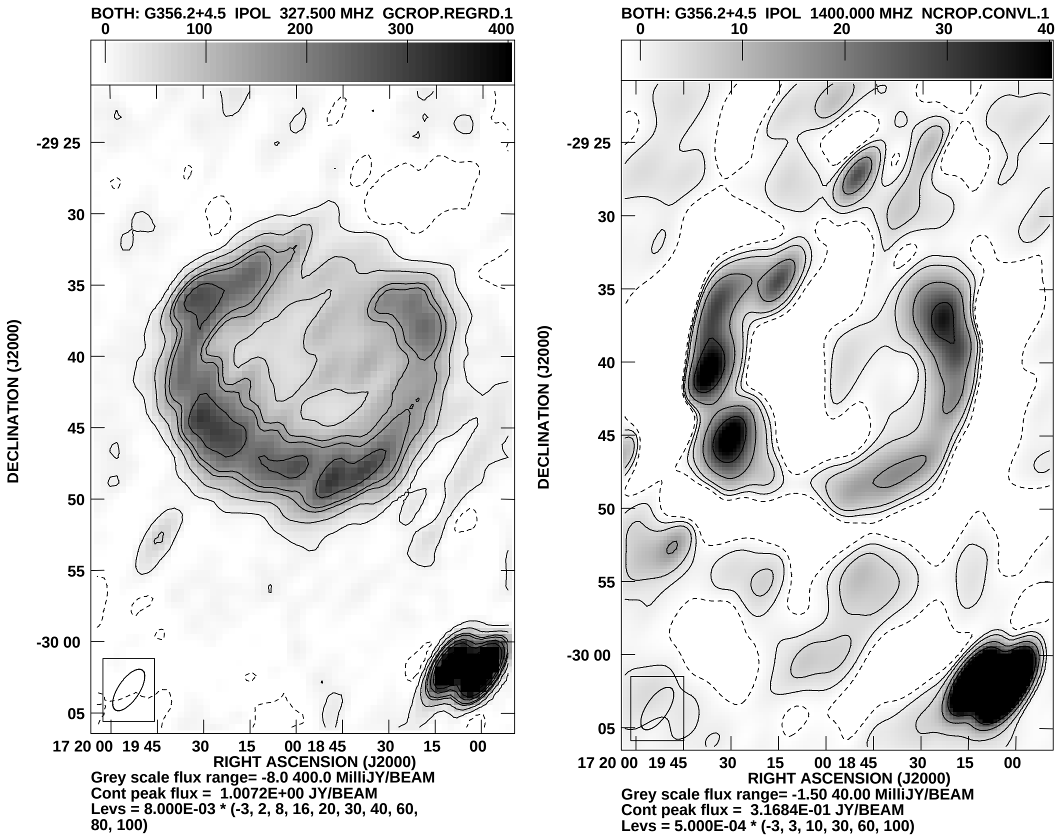

Figure 5.10: The GMRT image of G356.2+4.5 at 327 MHz is shown in the right panel and NVSS image at 1400 MHz in the left panel. The resolution in the GMRT image is $3' \times 1.5'$ along PA $-34°$ and the RMS noise in the map is 10 mJy/beam. The NVSS image has been smoothed to the resolution of the GMRT image and has a RMS noise of 0.5 mJy/beam.

5.2.6 G356.2$+$4.5

Fig. 5.10 shows the GMRT 327-MHz and NVSS 1400-MHz images of G356.2+4.5 where a well defined circular shell of emission of size $25'$ is evident. The co-ordinates of the center of the shell are $\mathrm{RA}_{J2000} = 17^{\mathrm{h}}18^{\mathrm{m}}58^{\mathrm{s}}$, $\mathrm{Dec}_{J2000} = -29°40'$. The RMS noise in the GMRT map is 10 mJy/beam. Low-level emission is seen projected against the central region. The NVSS image is shown in the right panel of Fig. 5.10. The SNR appears to be of shell-type morphology in both maps. The larger scale emission could be missing in the NVSS map due to poorer short spacing uv-coverage, plus the poorer overall uv-coverage of snap-shot observations.

There is significant variation in the brightness along the shell seen in both the 327- and 1400-MHz maps. Although there is a broad correlation between these variations at both frequencies, there are significant differences too. The gap in the emission seen to the south-east of the ring in the NVSS image is also seen in the PMN survey image (Duncan et al. 1997b). However it is filled with prominent emission in the 327-MHz GMRT image. These variations in the morphology could imply variations in the spectral index around the ring. The integrated flux density for this SNR at 327 MHz is 8.1 ± 1.7 Jy. The integrated flux density at 2.4 GHz was reported to be 3.0 ± 0.3 Jy and the value at 4.85 GHz from the PMN image was found to be 1.48 ± 0.13 Jy. This gives a spectral index of -0.66 ± 0.17 ($S \propto \nu^{\alpha}$). We did not use the total flux density from NVSS to determine the spectral index because of the missing emission in this image.

The presence of pulsar PSR B1717-29 in the field was noted by Duncan et al. (1997b). The Taylor et al. (1993) pulsar catalogue provides a characteristic age for this pulsar of 7.12×10^{6} yr and a dispersion measure of 42.6 ± 0.4 pc cm^{-3}. Using the Taylor & Cordes (1993) model for the electron density distribution in the Galaxy, the derived distance to the pulsar is 1.4 kpc, placing it just in front of the Sagittarius arm.

5.2.7 G358.0$+$3.8

Fig. 5.11 shows a $37' \times 39'$ region of emission, roughly circular in morphology with marginally brightened ring, whose emission closer to the plane, namely the south-eastern part is significantly brighter than on the opposite side. The morphology appears to be that of a shell-type SNR. Again there is broad correlation between the emission at 1400 and 327 MHz along the ring, though with significant detailed differences. Although the signal-to-noise ratio in both maps is low, there is good morphological correlation between the 327-MHz image and 4.85-GHz image from the PMN survey presented by Duncan et al.

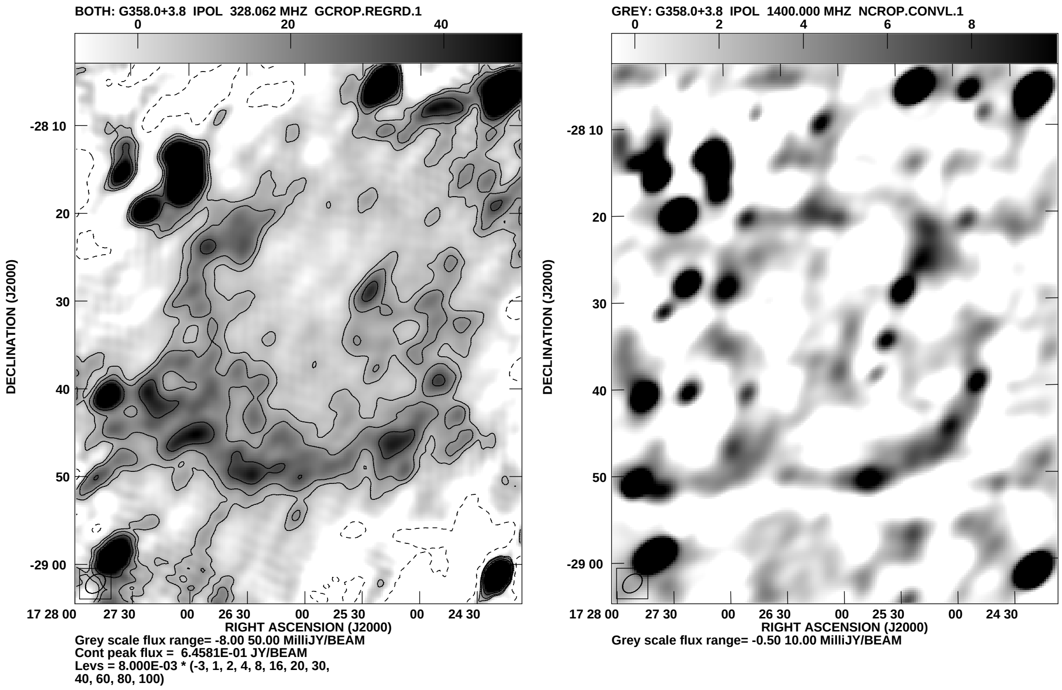

Figure 5.11: GMRT image of G358.0+3.8 at 327 MHz and NVSS image at 1400 MHz. The resolution in the GMRT image is $2.6' \times 1.8'$ along PA -48° and the RMS noise is 15 mJy/beam. The NVSS image has been smoothed to the resolution of the GMRT image and has a RMS noise of 0.5 mJy/beam.

at a comparable resolution. Brightening of the eastern arc is seen in both the images, while the rest of the ring is fainter. The integrated flux density at 2.4 GHz for this SNR was reported to be 2.4 ± 0.4 Jy, with a peak flux density of 400 mJy/beam. The value at 327 MHz is 2.5 ± 1.3 Jy and 0.79 ± 0.15 Jy at 4.85 GHz from the PMN image. Given the large angular size of this SNR, it is possible that some flux density may be missing in the GMRT image at 327 MHz. Duncan et al. (1997b) also noted that the 2.4-GHz emission might include a thermal component and therefore the flux densities at 2.4 and 4.85 GHz might be over estimated. Because of all these uncertainties, we did not compute the spectral index for this SNR. The co-ordinates of the center of the shell are ($\mathrm{RA}_{J2000} = 17^{\mathrm{h}}26^{\mathrm{m}}03^{\mathrm{s}}$, $\mathrm{Dec}_{J2000} = -28^\circ 36'$).

Note that the south-east protrusion seen in the GMRT image coincides with faint emission in the form of a smaller arc at the same location in the NVSS map, suggesting either the presence of another faint SNR in the field or a bi-annular morphology. Higher resolution, more sensitive mapping of this region is required to evaluate this possibility.

5.3 Continuum flux densities of known SNRs

With a $1^\circ.4$ field of view of GMRT at 327 MHz, there were other known SNRs in some of the fields. Many of them have been mapped at 327 MHz using the VLA, but there were some for which these GMRT images constitute the first 327 MHz images at a resolution of ~ 1 arcmin or less, with an, RMS noise of 3-15 mJy/beam. This section presents the results and discussion for these known SNRs.

5.3.1 G003.7$-$0.2

This is a classic barrel shaped SNR, first reported by Gray (1994a) where it was classified as a SNR based on the morphology alone. Gaensler (1999) mapped this at 1.4 GHz using the VLA in `CnD` and `BnC` array configurations and established the non-thermal nature of emission. This higher quality image at 1.4 GHz, and the 843 MHz image by Gray are in good agreement with the GMRT image at 327 MHz. The resolution in the GMRT image, shown in Fig. 5.12, is $20 \times 10\ \mathrm{arcsec}^2$, almost the same as that in the 1.4 GHz (Gaensler 1999). In all these images, this SNR satisfies the criterion used by Gaensler (1998) to classify it as a barrel shaped SNR. It has a clear ridge where there is practically no emission, even at the lowest frequency, which defines the axis of symmetry. It also has a clear point of maximum emission, almost perpendicular to the axis of symmetry.

The flux density in the GMRT 327-MHz image was found to be 4.5 ± 0.3 Jy. The flux density at 1.4 GHz is 1.7 ± 0.1 Jy and that at 843 MHz is 2.4 Jy, giving a spectral index of -0.66 ± 0.04. The spectral index listed in Greens catalogue (Green 2000)[2] is -0.65.

5.3.2 G355.9$-$2.5

This SNR, first identified by Clark et al. (1973) using 408 MHz and 5 GHz observations, is listed as a “distorted shell, brightest towards the south-east” in Green’s catalogue (Green 2000) with a spectral index of -0.5 and a size of 13 arcmin. The flux density at 408 MHz (resolution of 3 arcmin) is reported to be 12.3 Jy while at 5 GHz (resolution of 4 arcmin) the value is 3.4 Jy. The highest resolution image made by Dubner et al. (1993) using VLA at 1.4 GHz confirms this general morphology. Polarization observations by these authors

[2] Available from http://www.mrao.cam.ac.uk.surveys/snrs on the web

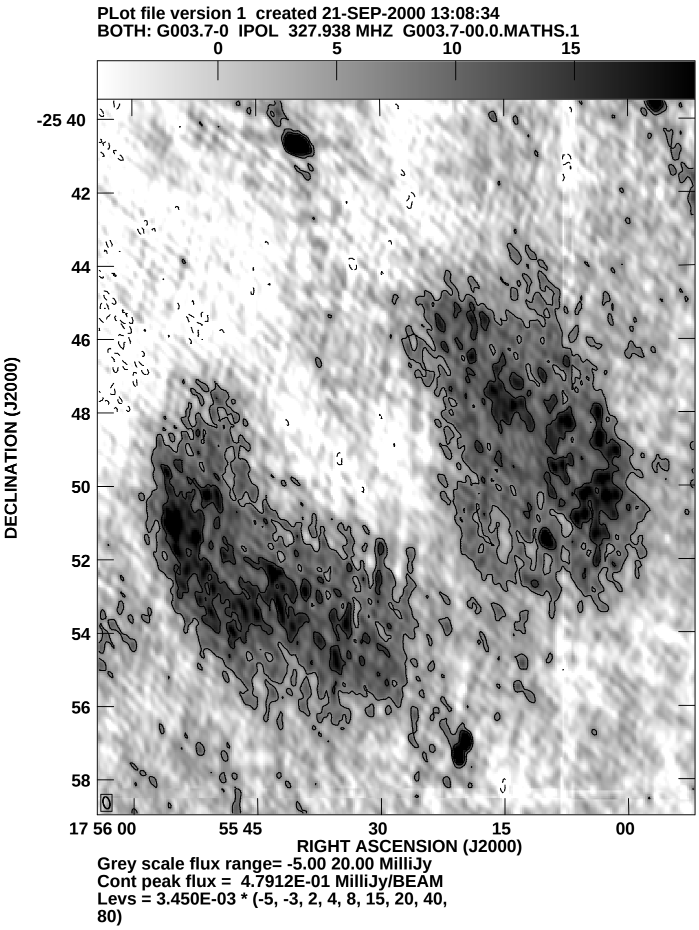

Figure 5.12: GMRT 327-MHz image of G003.7−0.2. The resolution in the image is $\sim 20 \times 10\,\mathrm{arcsec}^2$ and the RMS noise ~ 5 mJy/beam. The extended emission "breaks up" possibly due to a combination of uncorrected phase errors and the well known problem of deconvolution of extended sources using the CLEAN algorithm.

at 1465 MHz indicate significant linearly polarized intensity with a mean fractional polarization of 6% with the brightest region also most strongly polarized. Weaker emission, towards the east appears to complete the shell.

Gray (1994b) published a MEM deconvolved image at 843 MHz and measured a flux density of 6.5 Jy, a good 24% lower than expected from a source of spectral index of -0.5. The flux density of 5.0 Jy at 1465 MHz is also 21% lower than expected. The authors attribute this discrepancy to the missing extended flux in interferometric images.

The GMRT image at 332 MHz is shown in Fig. 5.3.2. In this pointing, this source lies at half power point of the primary beam. The smallest uv-spacing from which the visi-

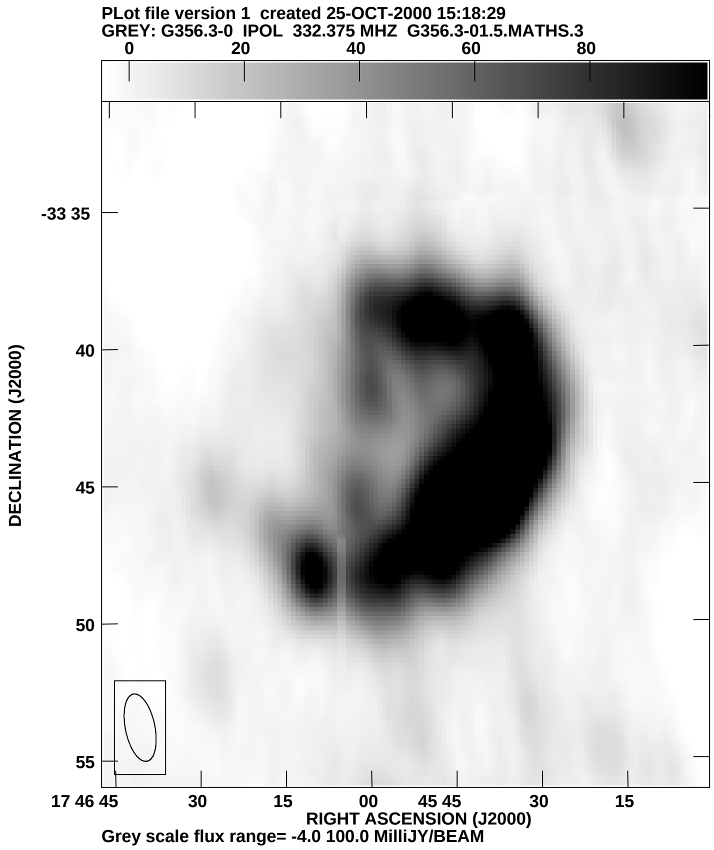

Figure 5.13: 327-MHz image of G355.9-2.5 using GMRT. The RMS noise in the image is about 10 mJy/beam and the resolution is $1.6' \times 0.8'$. This SNR lies on the very edge of the GMRT primary beam. The incomplete nature of the shell is apparent. However, there is an indication of weak emission in the east where the shell is incomplete. The vertical ridge passing through the middle is an artifact of combining different facets along the celestial sphere in a polyhedron imaging algorithm.

bility was reliably measured was about 90λ, corresponding to a largest angular scale of ~ 30 arcmin. The total angular size of this source is about 13 arcmin. Hence this source is not affected by the missing flux problem of interferometric images. A flux density of 14.2 ± 0.3 Jy was measured from the primary beam corrected image for this pointing, in close agreement with the expected flux density of 13.9 Jy at this frequency, corresponding to a spectral index of -0.5. The weak emission seen in the 1.4 GHz image is more clearly seen at 327 MHz and indeed there is a more complete shell than was seen at higher fre-

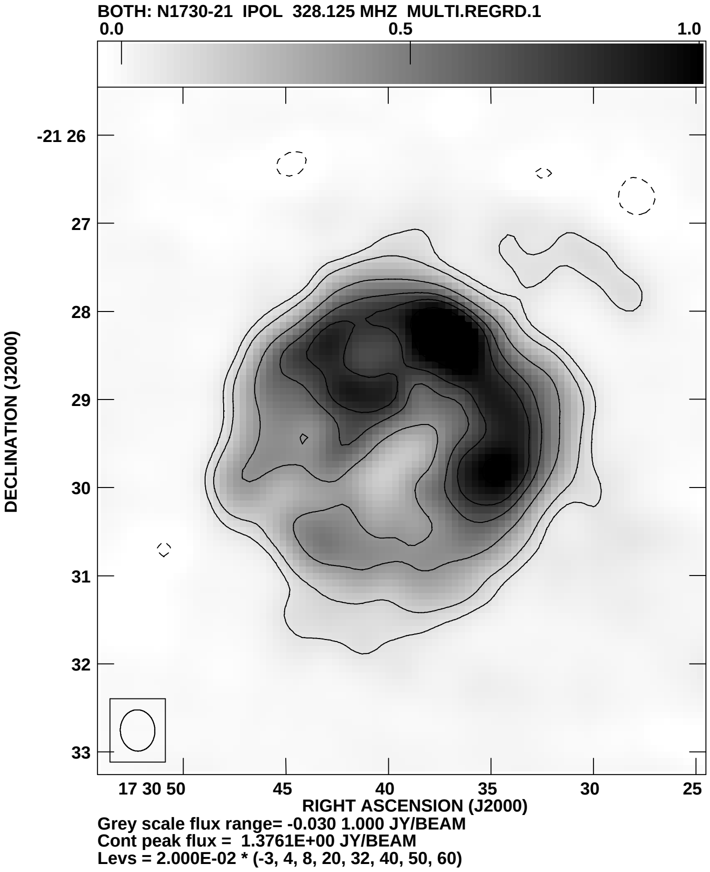

Figure 5.14: 327-MHz image of the Kepler's SNR (G004.5+6.8). The RMS noise in the image is about 25 mJy/beam and the resolution is 28×24 arcsec^2. The edge brightened morphology with the brighter norther rim (*away* from the Galactic plane) is clearly visible. The ridge running right across the SNR with small protrusions on either size is also clearly visible.

quencies.

The linear features noted by Gray in the 843-MHz image are also visible in this image. Although it is commented that these features are not seen in the 1465-MHz image (Dubner et al. 1993), they are clearly seen in the polarized intensity and although weak, can also be identified in the total intensity at this frequency. The spectral index of these features is probably then not very different from the rest of the source; there may be the usual filaments seen in many other SNRs.

5.3.3 Kepler's SNR (G004.5+6.8)

The field of G004.8+6.2 contains the well known shell-type Kepler's SNR of angular size 3 arcmin. A higher resolution image of this field was made, for the purpose of imaging this SNR at 327 MHz at the highest possible resolution. This higher resolution, primary beam corrected image is shown in Fig. 5.14. This is the only map known to me at 327 MHz at a resolution comparable to that at higher frequencies. The edge brightened shell towards the north is clearly visible. The morphology in this 327-MHz image is similar to that seen in the 1.4 and 5 GHz VLA images (Matsui et al. 1984). The distance to this SNR is estimated to be between 4.8 and 6.4 kpc from HI absorption and emission profiles (Reynoso & Goss 1999). The ridge running right across the SNR with small protrusions on both sides is also visible in the image. The integrated flux after primary beam correction is $\sim 38.4 \pm 0.5$ Jy. This SNR is also an X-ray source and Matsui et al. (1984), in a study of correlation between X-ray morphology and de-polarization between 1.4 and 5 GHz, have shown that there is a mixture of thermal and non-thermal gas associated with this SNR. High resolution imaging of other X-ray loud SNRs in radio and X-ray bands will be useful in determining if this is more generally true for other objects of this class.

5.4 Discussion

Observations of new candidate SNRs at 327 MHz, presented here, confirm these objects as SNRs on the basis of their morphology seen clearly at resolutions of $1'$ or less, as well as based on the non-thermal nature of emission and absence of thermal emission in the 60μm IRAS images. Only one of the objects (G004.2−0.0) is not detected at 327 MHz at the resolution required to decipher its morphology. There is also significant emission in the IRAS image at its location, implying the presence of thermal emission. At lower resolution, a 100-mJy, unresolved sources is detected, at the location of this object. The estimated flux density at 843 MHz is between 100 and 200 mJy. The existing radio flux densities and emission at IR band are therefore consistent with this source being a flat spectrum thermal source.

The morphology of some SNRs has long been suspected to be shaped by their interaction with nearby molecular clouds. Recently it has been argued that the OH (1720 MHz) emission is a good tracer of this interaction (Frail et al. 1994). The OH (1720 MHz) maser emission is distinguished from the OH maser emission at 1665, 1667 and 1612 MHz by the former being positionally and kinematically associated with SNRs while the latter are associated with HII regions. Both theoretical and observational evidence (Reach & Rho 1998, 1999; Frail & Mitchell 1998) suggest that the OH (1720 MHz) masers are associated with C-type shocks and are collisionally pumped in molecular clouds at temperatures and densities of $50 - 125$ K and $10^5 - 10^6$ cm^{-3} respectively (Lockett et al. 1999, and references therein). OH masers at 1665, 1667 and 1612 MHz cannot be produced under these physical conditions and the absence of these lines in observations which detect the OH (1720 MHz) line favors this interpretation. Measurements of the post shock density and temperature for IC443 (van Dishoeck et al. 1993), W28, W44 and 3C291 (Frail & Mitchell 1998) are in excellent agreement with these theoretical predictions. A solution to the problem of producing OH, which is not directly formed by shocks, is proposed by Wardle et al. (1999). They suggest that the molecular cloud is irradiated by X-rays produced by hot gas in the interior of the SNR. This leads to photo-dissociation of the H_2O molecules, which are produced by the shock wave in copious amounts, behind the C-type shock resulting into the required enhancement of OH just behind the C-type shock. The observed association of OH (1720 MHz) with X-ray-composite SNRs (i.e, SNRs with a shell-type radio morphology and a filled centre morphology in X-ray) and strong correlation between the morphology of the molecular gas and synchrotron emitting relativistic gas (Frail & Mitchell 1998) offers observational evidence for the hypothesis that the OH (1720 MHz) maser originates in post-shock gas, heated by the SNR shock passing through dense molecular cloud.

If the extended OH (1720 MHz) emission seen towards G001.4−0.1 (Yusef-Zadeh et al. 1999) is due to the SNR driving a C-type shock in a molecular cloud, one would expect the OH (1720 MHz) emission to be morphologically and kinematically associated with the general morphology of the radio continuum emission. The detection of a clear arc in the radio continuum image and the remarkable correlation with the OH (1720 MHz) emission towards this source is suggestive of such a model. If this association is true, the arc of emission is the boundary of the C-type shock driven in the molecular cloud by the SNR. The absence of any such cloud on the north eastern side of this SNR can explain the incomplete arc seen in the radio continuum as well as the OH (1720 MHz) emission. Also, the similarity of the radio morphology of this SNR, with G000.9−0.1, which is known to be a X-ray-composite SNR, further suggests that this SNR may also be of the X-ray-composite class. Interestingly, an X-ray source designated as `1RXS J175017.6-274646`, is detected in the ROSAT All-Sky Survey Faint Sources catalogue about 10 arcmin away. An alternative explanation for the correlation between the OH (1720 MHz) and radio continuum emission is that the maser emission is excited in the intervening material by the background emission of the SNR, having a similar origin as in the widespread OH (1720 MHz) emission in the Galactic plane (Haynes & Caswell 1977; Turner 1982). However, as pointed out by Yusef-Zadeh et al. (1999), the absence of any reported OH (1720 MHz) absorption line, the correlation of OH (1720 MHz) and radio continuum emission and the coincidence of the compact and extended OH (1720 MHz) emission argues against this alternative. Determination of the radio spectra of the shell and the central source and X-ray observations of this SNR would be future useful observations to determine the nature of this SNR.

G003.6−0.1, located about 8 arcmin west of G003.7−0.2 appears in the field of view of the GMRT 327-MHz observation as well as at 1.4 GHz VLA observations by Gaensler (1999). This source is detected in the 60μm IRAS image as well as at 2.7, 4.9 and 14.8 GHz and is discussed in greater detail in Chapter 6.

Barring G356.3-1.5, which appears to be barrel shaped, all others are shell-type SNRs. All these shells (and the rims for G356.3-1.5) are well resolved and show significant variations in the brightness along the shell. Caswell & Lerche (1979) proposed a correction to the $\Sigma - D$ relation (Clark & Caswell 1976; Case & Bhattacharya 1998, and references therein), by correcting for the variation in the ISM density away from the Galactic plane. They used the variation of the brightness across SNRs with respect to the Galactic plane to estimate the scale height of the ISM and derived the $\Sigma - D - z$ relation. In their sample, $\sim 25\%$ of SNRs show enhanced emission towards the Galactic plane which they attribute to the variation of the ISM density as a function of the distance from the Galactic plane. However, 5 of the 13 SNRs which did show asymmetry, were brighter *away* from the plane leaving the statistical significance of this result in serious doubt (Green 1984). Except for G355.9−2.5, G356.2+4.5 and G358.0+3.8, all the objects presented here, also show an enhancement in the brightness away from the Galactic plane ($\approx 30\%$) hinting that brightness variations across SNRs might be dominated more by local effects (interaction with the ISM, variations in the local ISM density, interaction with nearby molecular clouds, etc.) rather than a more global effect. It is also curious that in the current data set, all sources in the fourth quadrant of the Galaxy show an enhancement in the emission towards the plane. This new data plus higher resolution data for known SNRs which has now become available can be used to re-evaluate the $\Sigma - D - z$ relation. The current sample of SNRs for which higher resolution images better resolve the structure better is significantly larger than that available to Caswell & Lerche (1979).

With the exception of Cas-A and a handful of other remnants, few SNRs have reliably determined spatially resolved spectral index maps. A reliable continuum spectral index is an indirect measure of the relativistic electron energy spectrum. Simple Fermi shock acceleration theory predicts a spectral index of -0.5, consistent with many shell-type SNRs. However, this inconsistent with substantially higher values of the spectral index, reliably measured for only a few SNRs. Reynolds & Ellison (1992) successfully reproduced the observed radio spectra for Tycho's and Kepler's SNRs by invoking self-consistent, nonlinear shock model of first-order Fermi acceleration. Such models predict a slightly concave spectrum and can also estimate the mean magnetic field, if the precise shape of the lower frequency spectrum is known.

The GMRT covers the low frequency range between 100 MHz and 1 GHz in 4 bands at 150, 233, 327 and 610 MHz and can also be used to observe at 1060 MHz. With a resolution of ~ 20 arcsec at the lowest frequency to ~ 2 arcsec at the highest frequency, the GMRT can be used most effectively to determine the low frequency integrated spectra for most of the SNRs in the Galaxy and potentially remove the '?' (indicating that the quoted number is not reliable) from the quoted spectral indices in the SNR catalogue (Green 2000).

The GMRT frequency coverage is also well suited to the separation of sources of thermal and non-thermal emission. Emission from a typical Galactic thermal sources have a flat spectra above ~ 1 GHz. Below 1 GHz, the emission progressively decreases, with a typical spectral index of 2.0. The spectrum of a typical Galactic SNR has a negative spectral index (typically -0.5) above about 100 MHz and turns over below this frequency due to free-free absorption (see Fig. 5.15). The frequency range from 100 MHz to about 1 GHz is therefore very well suited to distinguish between thermal and non-thermal emission in the Galaxy. At the range of frequencies available at the GMRT, the distinction between the typical thermal and non-thermal spectra is most pronounced. With the high angular resolution provided by the GMRT, multi-frequency GMRT observations in the Galactic plane will easily distinguish between thermal and non-thermal sources as well as separate superimposed thermal and non-thermal components and help in identifying compact SNRs which may have been classified as thermal sources due to lack of resolution.

Measurement of a low frequency turnover below 100 MHz in the integrated spectrum of a sample of SNRs, due to free-free absorption, is a powerful probe of the distribution of low density ionized gas in the ISM, providing continuum optical depths towards various lines of sight in the Galaxy. It has been suggested that this same low density gas gives rise

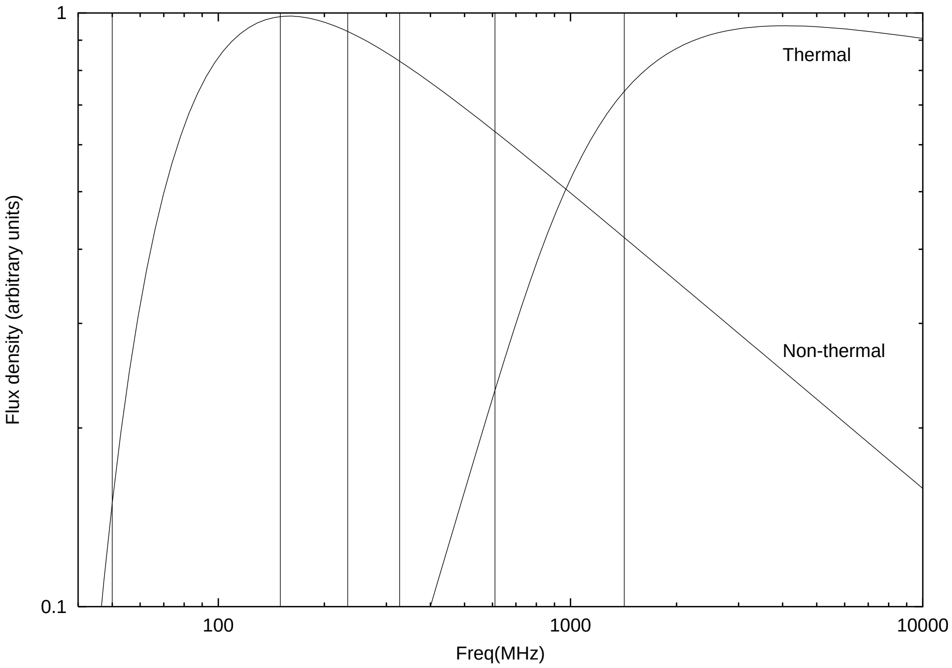

Figure 5.15: Comparison of typical spectra of Galactic SNRs and HII regions (thermal and non-thermal respectively). The first vertical line corresponds to 74 MHz (now available for observing with the VLA). Other vertical lines mark the GMRT frequency bands. GMRT covers the region of the spectra best suited for separating thermal and non-thermal sources in the Galaxy.

to low frequency RRLs which have been detected in almost every direction in the inner Galaxy (Kassim 1989). The detection of low frequency RRLs (Roshi & Anantharamaiah 2000) suggests (Anantharamaiah 1985b, 1986) that this same gas may be the low density extended HII envelope (EHEs) surrounding higher density HII regions. However, past low frequency observations have had insufficient resolution to study individual cases in sufficient detail to confirm this physical picture. The detection of spatially resolved continuum absorption against SNRs using the VLA at 74 MHz and using the GMRT and/or the VLA at 327 MHz for RRL observations will make significant advances in this area and resolve a long standing and important question.

A large number of known SNRs will be well resolved by the GMRT at all GMRT frequency bands. The spectral index of the radio emission changes across the SNR, giving information about the radiation and electron acceleration mechanism as well as about the interaction with the ISM. Apart from morphology, the difference in the spectral index between the Plerionic emission (filling the central portion of the SNR) and the emission from the shell is crucial in identifying filled-center or composite SNRs. Both the low frequency integrated spectral index as well as high resolution images of these SNRs, will be very useful for statistical studies of Galactic SNRs, as well as for the studies of the interaction of individual SNRs with the local ISM. For many of these SNRs, such observations will also be the first observations below 1 GHz and often the first observations below 2.4 GHz. The GMRT primary beam at 1420 MHz has a FWHM of 25 arcmin. Hence, SNRs of size ≤ 15 arcmin can be easily observed for HI absorption to estimate the kinematic distance using the Galactic rotation model.

Strictly speaking, spectral index maps can be reliably made only when the spatial frequency coverage at different frequencies is identical (or close to it). However, one can determine the average spectral index at different positions across the SNR via the "T-T plots" successfully used by Anderson & Rudnick (1993) to generate spectral index maps for G039.2−0.3 and G041.1−0.3. Essentially, the local gradient of the emission at two frequencies is used to measure the local (average) spectral index eliminating the error due to differing constant offset between images due to differing spatial frequency coverages. Such spectral index maps, although at a lower resolution, provide information needed to relate the observed spectral properties to the local dynamical situations in individual SNRs. Recently, Katz-Stone & Rudnick (1995) and others have used the technique of spectral tomography to study the spectral variations within the Tycho's SNR (Katz-Stone et al. 2000b).

All these observations can be done with the GMRT in the current state. This dissertation has extensively used the 327-MHz band and a RMS noise of about ≤ 10 mJy/beam has been regularly achieved. RMS noise of few mJy/beam has also been achieved at 1420-MHz band and 610 MHz bands. The imaging performance at 233 and 150 MHz is yet to be established with some careful data analysis. Therefore, as a future extension of this work, the above mentioned observations should be done with the GMRT.